JTTEE5 14:462-470
DOI: 10.1361/105996305X76432
1059-9630/$19.00 © ASM International

Peer Reviewed

Implementation and Development of the Incremental Hole Drilling Method for the Measurement of Residual Stress in Thermal Spray Coatings

T. Valente, C. Bartuli, M. Sebastiani, and A. Loreto

(Submitted October 26, 2004; in revised form July 25, 2005)

The experimental measurement of residual stresses originating within thick coatings deposited by thermal spray on solid substrates plays a role of fundamental relevance in the preliminary stages of coating design and process parameters optimization. The hole-drilling method is a versatile and widely used technique for the experimental determination of residual stress in the most superficial layers of a solid body. The consolidated procedure, however, can only be implemented for metallic bulk materials or for homogeneous, linear elastic, and isotropic materials. The main objective of the present investigation was to adapt the experimental method to the measurement of stress fields built up in ceramic coatings/metallic bonding layers structures manufactured by plasma spray deposition. A finite element calculation procedure was implemented to identify the calibration coefficients necessary to take into account the elastic modulus discontinuities that characterize the layered structure through its thickness. Experimental adjustments were then proposed to overcome problems related to the low thermal conductivity of the coatings. The number of calculation steps and experimental drilling steps were finally optimized.

Keywords hole drilling, integral method, plasma spray, residual stress

1. Introduction

Residual stress fields of variable intensity and distribution affect thermal-sprayed coatings as a consequence of their manufacturing process, always involving the high temperature deposition of a plastic material onto a cold, rigid substrate followed by a rapid cooling and modification of the mechanical properties of the deposited layers.

The quantitative determination of these stresses is an issue of great interest, especially for the preliminary stages of coating selection and design and for the subsequent phase of optimization of the manufacturing process parameters (Ref 1, 2).

The problem is complex and critical, as a direct consequence of the variety of critical parameters involved in the deposition process and in consideration of the fact that various non-independent sources of stresses are active in different stages of the production process.

Residual stress in a thermal-spray coating (Ref 3, 4) σ_c can be mainly described as the sum of two different contributions (Ref 3-6): the "quenching stresses" σ_q generated during the immediate contraction of individual lamellae deposited on a cold substrate, and the differential thermal contractions (DTC) stresses σ_{th} originating from differential thermal contractions of substrate and coating:

$$\sigma_c = \sigma_q + \sigma_{th} \quad \text{(Eq 1)}$$

In particular, quenching stresses arise from impact, spreading and solidification of each molten particle (at temperature T_m) on the substrate surface. They are always tensile and can be, in principle, approximately estimated by the following equation:

$$\sigma_q = E_c \int_{T_s}^{T_m} \alpha_c(T)\mathrm{d}T \quad \text{(Eq 2)}$$

where T_m = coating melting temperature, T_s = substrate temperature, α_c = thermal expansion coefficient, and E_c = elastic modulus of the coating.

Several sources of error, however, can affect Eq 2 (Ref 5): In the first place, elastic modulus of sprayed materials E_c is very different from that of the corresponding bulk materials E_b (with values of the E_c/E_b ratio as low as 1/10), mainly as a consequence of coating porosity and lamellar microstructure. Moreover, stress relaxation phenomena (Ref 5) (creep and yielding for metals, microcracking for ceramics) can be responsible for a remarkable decrease of the final value of quenching stress, especially in the case of brittle ceramic coatings (Ref 1, 5). As an example, a residual tensile stress of about 10 MPa can be experimentally evaluated by in situ curvature measurements for plasma sprayed alumina (Ref 5) while quenching stresses of the order of the GPa would be obtained by simply applying Eq 2.

Thermally induced stresses, on the other hand, result from misfit strains generated by DTC caused by thermal expansion

T. Valente, C. Bartuli, M. Sebastiani, and **A. Loreto,** Department of Chemical & Materials Engineering, University of Rome "La Sapienza," Via Eudossiana 18 - 00184 Rome RM, Italy. Contact e-mail: bartuli@uniroma1.it.

coefficients (CTE) mismatch between coating and substrate; in particular, DTC stresses are induced during the final cooling stage from processing temperature (T_s) to room temperature (T_r).

The equation correlating the mentioned misfit strains to the thermal properties of substrate and coating is as follows (Ref 5):

$$\Delta\varepsilon = \int_{T_r}^{T_s} [\alpha_c(T) - \alpha_s(T)]dT \quad \text{(Eq 3)}$$

where α_s is the coefficient of thermal expansion of the substrate.

Starting from Eq 3, residual stress can be evaluated, in the case of linear-elastic material behavior by simply applying the well-known Hooke's Law:

$$\sigma_{th} = \frac{E_c}{1-\nu_c}\int_{T_c}^{T_s} [\alpha_c(T) - \alpha_s(T)]dT \quad \text{(Eq 4)}$$

where ν_c is the coating Poisson's ratio. Equation 4 shows that for $\alpha_c < \alpha_s$, compressive thermal stresses arise in the coating due to final cooling after spraying. For a rough estimation of the order of magnitude of DTC residual stresses, Eq 4 can be approximated:

$$\sigma_{th} = \frac{E_c}{1-\nu_c}[\alpha_c(T_r) - \alpha_s(T_r)] \cdot (T_s - T_c) \quad \text{(Eq 5)}$$

Moreover, CTEs are a function of temperature, so that thermal stresses can also arise within individual layers if through-thickness thermal gradients are present. This is generally the case when the heat flux generated by the plasma torch is repeatedly transferred to the substrate and to the deposited layers during coating buildup.

Different experimental techniques are available for the direct measurement or indirect evaluation of residual stress (Ref 6-8): Among the most important are x-ray (Ref 9) or neutron (Ref 10) diffraction methods, layer removal method (Ref 11-16), and high-speed hole drilling techniques (Ref 10, 17-19).

The hole-drilling method (Ref 19), in particular, is a versatile technique widely used for the characterization of the stress fields in the most superficial layers of bulk metallic materials. The main objective of the present investigation was that of implementing and adapting the method to the experimental determination of the residual stress fields in plasma-sprayed composite structures consisting of a ceramic (alumina) top coat and an intermediate metallic bonding layer (Ni 20 Al).

A modification of the theoretical model was implemented to account for the discontinuity of elastic modulus along the coating-bond coat thickness. Experimental adjustments were also proposed to overcome problems related to the low thermal and electrical conductivity of the ceramic coatings.

2. Materials and Methods

2.1 Plasma-Sprayed Coatings

Metal-ceramic layered systems were used for the experimental evaluation of the residual stress field. Plasma-sprayed alumina coatings were deposited starting from commercially pure alumina powders (Metco 105NS, −325mesh +15 μm) (Sulzer Metco Holding AG, Winterthur, Switzerland) onto AISI 4037 carbon steel substrates, with interposition of a metallic Ni20Al bond coat (Metco 404NS powders, −170 + 270 mesh). Process parameters of the air plasma spray process used for the deposition of the ceramic top coat are summarized in Table 1.

Table 1 Operating parameters for APS deposition of the ceramic top coat

Parameter	Value
Substrate	Steel AISI 4037
Spraying distance	115 mm
Plasma gas, slpm	50 Ar, 12 H_2
Plasma current	560 A
Plasma tension	73 V
Number of torch passes	46
Cooling gas	4.5 bar
Total thickness	320 μm

Table 2 Comparison between calibration coefficient *B* calculated from the analytical solution and simulated by finite element analysis

Hole diameter, mm	*B* (exact solution)	*B* (simulated)	Error %
1.6	-7.1256×10^{-13}	-7.0434×10^{-13}	1.15
1.8	-8.7391×10^{-13}	-8.7101×10^{-13}	0.33
2.0	-1.0411×10^{-12}	-1.0432×10^{-12}	0.20
2.2	-1.2128×10^{-12}	-1.2161×10^{-12}	0.27
2.4	-1.3744×10^{-12}	-1.3043×10^{-12}	0.54

Ceramic coatings are characterized by an average thickness of about 320 μm and a total porosity of about 10% (as measured by image analysis of polished cross sections, Fig. 1); a dual phase microstructure of αAl_2O_3 and γAl_2O_3 was identified by x-ray diffraction. An average thickness of about 180 μm was measured for metallic bonding layers.

For the mechanical characterization of the ceramic coating, four-point bending tests were performed at room temperature. Specimens 3 × 4 × 50 mm were tested according to ASTM C1161-02c standard (Ref 20) by a MTS Bionix (MTS, Eden Prairie, MN) universal testing machine with a load cell of 25 kN. An average value of the elastic modulus *E* of 55 GPa with a standard deviation of 5 GPa was calculated for the alumina top coat on the basis of the classic beam theory. A value of 80-100 GPa was assumed for the bond coat.

2.2 Hole-Drilling Technique

The hole drilling strain gage technique (Ref 18, 19, 21-30) is a semidestructive method for the determination of residual stresses in the superficial layers of a solid body.

The technique simply consists of two stages: (1) removal of the stressed material by drilling a small hole (about 2 mm diameter) on the surface of the body, and (2) measurement of the relaxation strains occurring around the hole by means of an extensimetric rosette. Residual stresses are then calculated from the measured deformations by means of an analytical model based on the solution of the problem of the loaded wide plate with hole.

In the case of non-uniform through-thickness stresses, the test must be divided into several small depth increments, and the

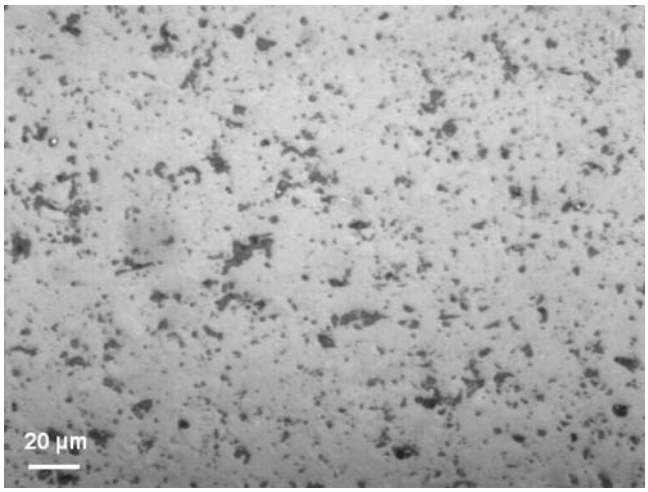

Fig. 1 Microstructure of an air plasma sprayed Al_2O_3 coating (polished cross section, optical microscope)

produced relaxation must be determined for every single incremental step.

A strain/depth curve can thus be plotted from experimental measurements, and can then be used to determine the residual stress through-thickness variation. The number of calculation steps used to determine the stress field with sufficient accuracy is selected on the basis of an optimization process and is generally smaller than the number of actual experimental steps of the test.

2.2.1 Fundamental Equations: The Integral Method. The analytical determination of residual stress from relaxation strains is based on the expression of the field of radial deformation originating around a through-thickness hole in an infinite plate subject to a generic tensile load.

The distribution of the radial relaxation strain ε_r generated by the hole is then analytically determined and can be expressed:

$$\varepsilon_r = A(\sigma_{max} + \sigma_{min}) + B(\sigma_{max} + \sigma_{min})\cos(2\alpha) \quad \text{(Eq 6)}$$

where α is the angle measured with the main direction 1 (Fig. 2).

In the case of an extensimetric rosette shown in the figure by considering an appropriate reference system, the correlation between the relaxation strains measured by the three strain gauges and the generic plane stress field (σ_1, σ_3, τ_{13}) can be expressed (Ref 21):

$$\begin{bmatrix} A+B & 0 & A-B \\ A & -2B & A \\ A-B & 0 & A-B \end{bmatrix} \begin{bmatrix} \sigma_1 \\ \tau_{13} \\ \sigma_3 \end{bmatrix} = \begin{bmatrix} \varepsilon_1 \\ \varepsilon_{13} \\ \varepsilon_3 \end{bmatrix} \quad \text{(Eq 7)}$$

by defining the following parameters:

$$p = \frac{(\varepsilon_3 + \varepsilon_1)}{2}; \quad q = \frac{(\varepsilon_3 + \varepsilon_1)}{2}; \quad t = \frac{(\varepsilon_3 + \varepsilon_1 - 2\varepsilon_2)}{2};$$
$$P = \frac{(\sigma_3 + \sigma_1)}{2}; \quad Q = \frac{(\sigma_3 + \sigma_1)}{2}; \quad T = \tau_{13} \quad \text{(Eq 8)}$$

Equation 8 can be simplified (Ref 21):

$$\begin{cases} AP = p \\ BQ = q \\ BT = t \end{cases} \quad \text{(Eq 9)}$$

The calibration coefficients A and B are analytically determined only in the case of through-thickness hole, and they cannot be analytically expressed as a function of known parameters in the case of a blind hole in the presence of a nonuniform through thickness stress. In this second case, coefficients A and B must therefore be calculated by calibration using finite element simulations.

The integral method (Ref 22) is the most widely accepted procedure for the analysis of non-uniform through-thickness stress: the relaxation strain $\varepsilon_i(h)$ along the non-dimensional hole depth h is expressed as the integral of the infinitesimal strain components deriving from the stress at the depth $0 \le H \le h$ (with h, H, and other geometrical parameters defined as in Fig. 3):

$$\begin{cases} p(h) = \int_0^h \bar{A}(H,h)P(H)\mathrm{d}H \\ q(h) = \int_0^h \bar{B}(H,h)Q(H)\mathrm{d}H \\ t(h) = \int_0^h \bar{B}(H,h)T(H)\mathrm{d}H \end{cases} \qquad 0 \le H \le h \quad \text{(Eq 10)}$$

where

$$\begin{cases} P(h) = [\sigma_3(H) + \sigma_1(H)]/2 \\ Q(H) = [\sigma_3(H) - \sigma_1(H)]/2 \\ T(H) = \tau_{13}(H) \end{cases}$$

$$\begin{cases} p(h) = [\varepsilon_3(h) + \varepsilon_1(h)]/2 \\ q(h) = [\varepsilon_3(h) - \varepsilon_1(h)]/2 \\ t(h) = [\varepsilon_3(h) + \varepsilon_1(h) - 2\varepsilon_2(h)]/2 \end{cases} \quad \text{(Eq 11)}$$

The influence functions, $\bar{A}(H,h)$ and $\bar{B}(H,h)$, (likewise calibration coefficients A and B), represent the relaxation strains per unit depth caused by the unit stress at the depth H, for a hole of depth h. The determination of the functions cannot be carried out analytically, and Eq 10 must therefore be discretized, dividing their calculation into n_c steps (Ref 23):

$$\begin{cases} \sum_{j=1}^{j=i} \bar{A}_{ij}P_j = p_i \\ \sum_{j=1}^{j=i} \bar{B}_{ij}Q_j = q_i \\ \sum_{j=1}^{j=i} \bar{B}_{ij}T_j = t_i \end{cases} \qquad 1 \le j \le i \le n_c \quad \text{(Eq 12)}$$

where the three unknown stress vectors, P_j, Q_j, T_j (defined as in Eq 8), can be determined starting only from the experimental values of relaxation strains p_j, q_j, t_j, in the n_c calculation steps after the finite element determination of the two calibration coefficient matrices.

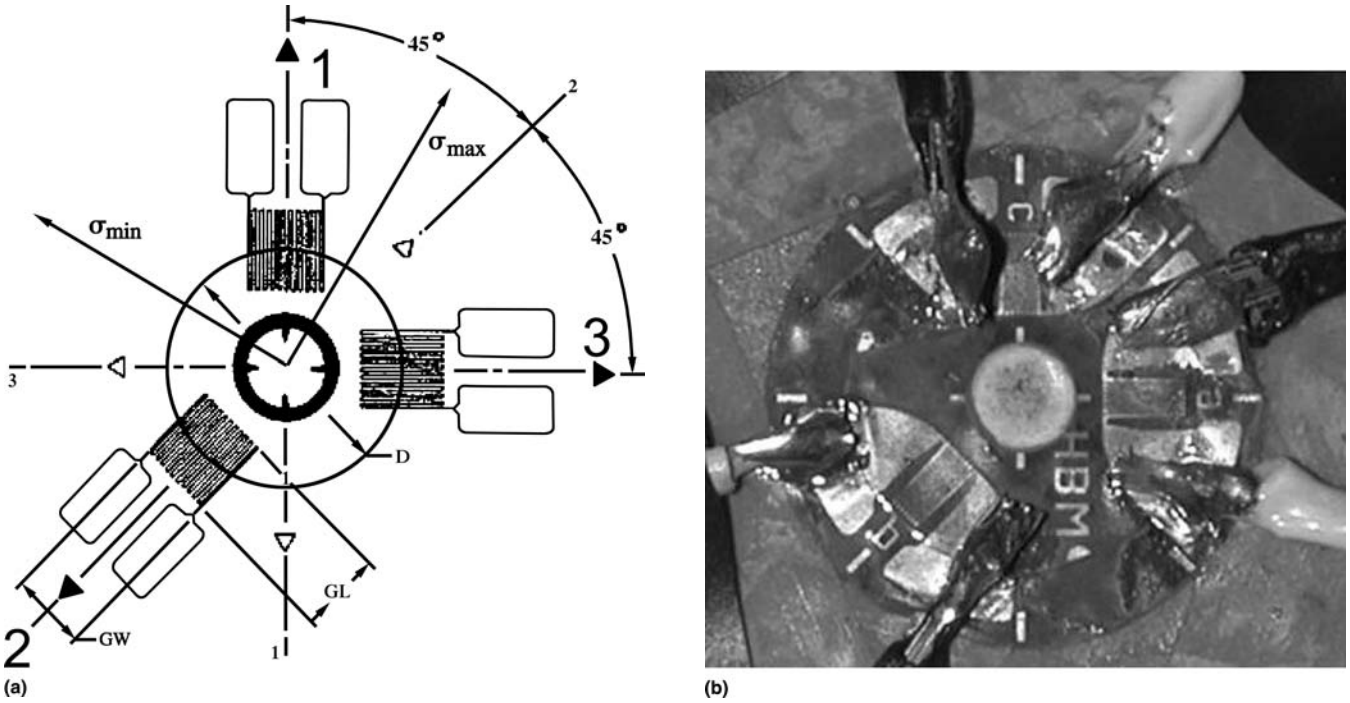

Fig. 2 Strain gauge rosette for the measurement of relaxation strains: (a) schematic representation with adopted reference system and (b) HBM RY61-1,5/120S rosette attached to the substrate, with central drilled hole

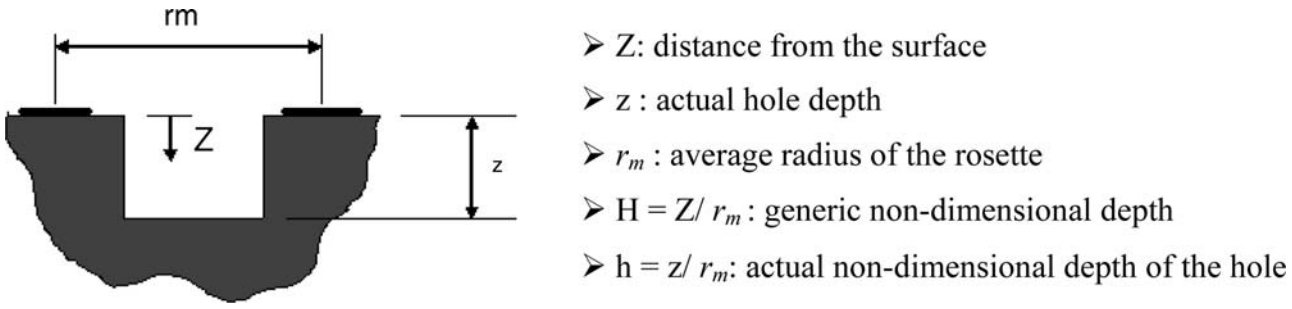

Fig. 3 Geometrical parameters for the definition of the integral method

The generic term A_{ij} represents the relaxation strain contribution given by the unit hydrostatic stress in the *j*th step when the hole depth is the sum of *i* steps, as described in Fig. 4. The coefficients B_{ij} are calculated by analogous procedure for pure shear stress.

3. Model Optimization

3.1 Calibration Coefficients for a Multimaterial System

In the case of bulk materials, calibration coefficients can be calculated independently of the type of material using appropriate interpolation procedures (Ref 22, 23). This simplification, however, cannot be adopted for multilayered systems, where discontinuities of the elastic modulus are experienced in correspondence with the coating-bonding layer-substrate interfaces. Moreover, calibration coefficients must be calculated for every individual combination of coating/bond-coat/substrate thickness.

The finite element model for the determination of the calibration coefficients was implemented using the calculation code ANSYS 7.0. The adopted geometrical model consists of a plane disk with a diameter slightly larger than that of the extensimetric rosette (Fig. 5).

The mesh definition of the area immediately surrounding the hole was the critical step in the realization of the model. A very fine and regular mesh was defined around the hole (Fig. 5a), while increasingly larger volume elements were selected for increasing distance from the hole center. On the right hand of the model illustrated in Fig. 5(a), showing the coating/bond-coat/substrate composite system, the location of the strain gauge used for the calibration can also be observed. Figure 5(b) details the geometrical model adopted for the calculation of the A_{32} coeffi-

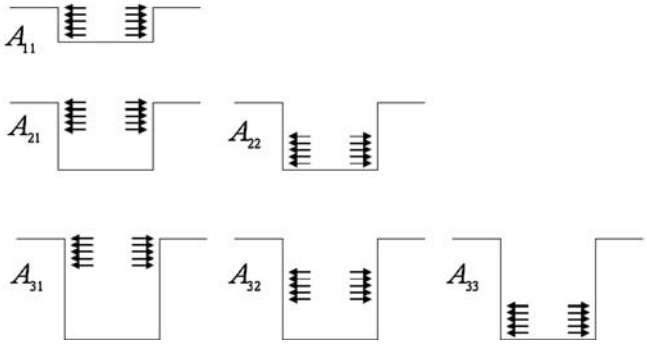

Fig. 4 Representation of the significance of the calibration coefficients A_{ij}

cient: the hole is 3 steps deep, and the calibration stress is applied on the second step.

The developed program uses an input Fortran file implementing an ANSYS cycle giving as an output file the two calibration coefficient matrices adapted for the coating system and for the examined calculation steps distribution.

Discontinuities of the elastic modulus through the system thickness can be properly taken into account, with the only simplifying hypothesis of perfect adhesion between the different layers.

Moreover, the number and distribution of the calculation steps can be selected without restriction, which is very important for the minimization of the stress calculation error, as will be pointed out in the next paragraphs.

3.2 Hole Eccentricity

In experimental practice, it is virtually impossible to drill a perfectly centered hole inside the strain gauge rosette. The hole eccentricity (schematically shown in Fig. 6 [Ref 26]) can be the cause of an error in the calculation of the residual stress (Ref 26-29); such source of inaccuracy can be minimized by developing suitable corrective factors determined on the basis of the deformation field originated around the hole. The problem was analytically solved by Vangi (Ref 26) for the case of uniform through-thickness stress. In particular, the fundamental expressions of the integral method are modified by correlating the radial strain measured in the generic point O_i when the hole is centered in O′ with the residual stresses calculated according to the reference system (X_3Y_3):

$$\{\varepsilon_i\} = \left\{\frac{1}{E}, -\frac{\nu}{E}, 0\right\} \begin{bmatrix} 1 & 0 & 0 \\ 0 & \cos(-2\alpha_i) & \sin(-2\alpha_i) \\ 0 & -\sin(-2\alpha_i) & \cos(-2\alpha_i) \end{bmatrix} [a]_i \begin{bmatrix} 1 & 0 & 0 \\ 0 & \cos(2\zeta_i) & \sin(2\zeta_i) \\ 0 & -\sin(2\zeta_i) & \cos(2\zeta_i) \end{bmatrix} \begin{Bmatrix} P \\ Q \\ T \end{Bmatrix} \quad \text{(Eq 13)}$$

where α_i and ζ_i (Fig. 6) are the geometrical parameters characterizing the eccentricity, easily correlated analytically to the experimentally measured terms e and β, and $[a]_i$ represents the correspondent term of the calibration coefficients matrix previously calculated by finite element simulation. Equation 13 can then be further modified (Ref 26) and adapted to the case of variable through thickness stress.

3.3 Calculation Steps

Several recent studies (Ref 23, 25, 30) have demonstrated that the choice of the number and distribution of the calculation steps can strongly influence the error affecting the residual stress determination.

According to the general principle of de Saint Venant, it can in fact be assumed that the determination of the relaxation strains generated by residual stresses at higher depth are affected by errors larger than those relative to strains originating from more superficial stresses. Therefore, very large errors (up to several orders of magnitude) can be experienced by dividing the total depth in numerous calculation steps of limited constant depth.

A first approximate solution was proposed (Ref 23) and consisted of steps of increasing width for increasing hole depth, thus attributing an approximately equivalent weight to the error in the stress at various depth. A more rigorous investigation (Ref 25) has demonstrated that the optimal condition, determined by minimizing the mathematical expression of the error, is obtained by limiting the calculation steps to a maximum of 10, and by optimizing their distribution in such a way that the terms of the main diagonal of the two calibration coefficient matrices are equal:

$$A_{nn} = \text{constant} \quad 1 \le n \le n_c$$
$$B_{nn} = \text{constant} \quad 1 \le n \le n_c \quad \text{(Eq 14)}$$

Seven calculation steps were selected for the experimental project described in the present work, with a depth distribution optimized by applying Eq 14, as suggested in Ref 25. It must be again pointed out that the number of calculation steps does not correspond to the number of experimental drilling steps; in particular, the hole drilling procedure was divided into the highest possible number of steps (20 steps for the present investigation), and experimental strain measurements were performed at each step; the plotted strain/depth values were then interpolated in continuous $\varepsilon\backslash h$ curves (as illustrated in the next paragraphs), used for the calculation of the actual values of stresses along the hole depth.

4. Experimental Procedure

Experimental tests were carried out using the Restan 44 drilling machine (Sint Technology, Calenzano, F1, Italy) shown in Fig. 7, allowing for precise centering of the end mill by means of a coaxially assembled optical microscope and for the direct measurement of the hole diameter and eccentricity by means of a centesimal dial gauge.

The mill is powered by a compressed air turbine (p = 5 bar, ω = 350,000 rpm), and vertical displacement is generated by a stepper motor and electronically controlled for single feed motion steps of 1 μm. The whole device is mounted and magnetically fixed to a metallic table. The position of the end mill on the surface of the sample is controlled by an electric circuit, responding to the electric contact between the tip of the end mill and the conductive sample.

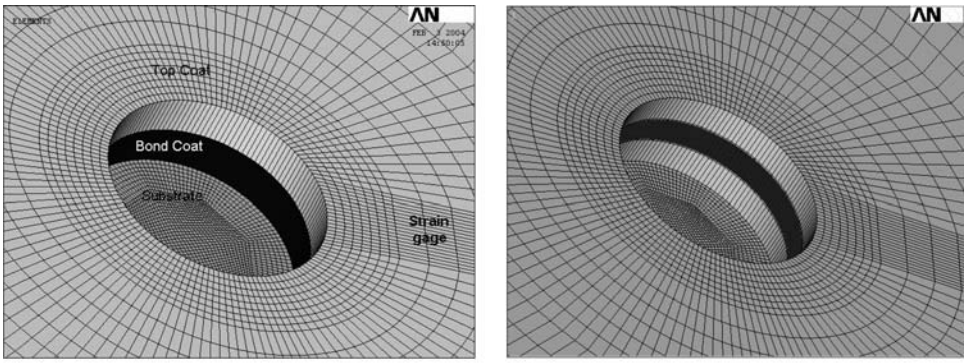

Fig. 5 Geometrical model adopted for the calculation of the calibration coefficients in the area surrounding the drilled hole (ANSYS software): (a) identification of substrate, bond-coat, top-coat and strain gauge and (b) detail for the calculation of the A_{32} coefficient

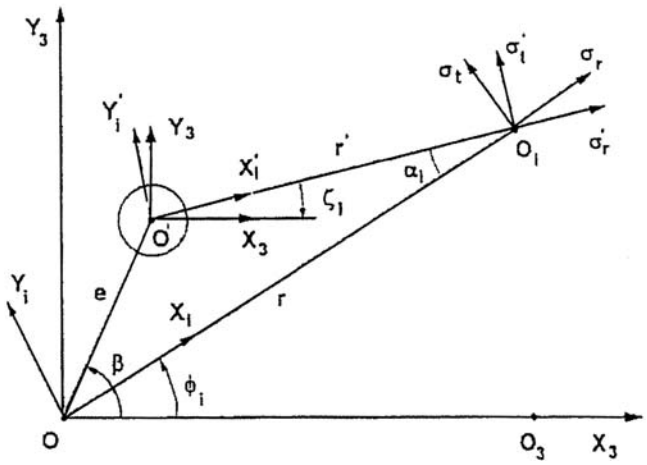

Fig. 6 Schematic representation of an eccentric hole (from Ref 29): Notations for the hole-rosette geometry in the presence of eccentricity between the center of the hole (O′) and the center of the rosette (O)

To allow for the correct functioning of the end mill positioning system also in the case of insulating ceramic materials, alumina top coats were previously gold sputtered (Edwards Sputter Coater) (BOC Edwards, Crawley, West Sussex, UK) and thus made superficially conductive without altering the residual stress state in the samples.

The low thermal conductivity of the coatings is also responsible for a severe sample heating on drilling, too intense to be simply accounted for by means of thermal balance strain gages. A minimum cooling time of 100 s between individual drilling steps was therefore selected to allow for complete cooling before the measurement of the strain.

The hole drilling technique can easily achieve depths of about 1 mm; however, inaccuracy of the results strongly increases for increasing depths of the analyzed layers. The analysis was therefore limited to the residual stress fields within the ceramic top coat, with a total depth of about 300 μm.

The relaxation strains measured for the 20 drilling steps in the depth range of 20-320 μm are plotted in Fig. 8 and interpolated with algebric polynomial functions of the sixth degree. After the

Fig. 7 Hole drilling RESTAN apparatus: An optical microscope is mounted coaxially to the end mill, and a centesimal dial gauge serves for the measurement of hole eccentricity.

evaluation of the hole diameter and eccentricity, residual stresses can be calculated and results interpreted.

5. Results and Discussion

As a preliminary validation of the finite element model for the calculation of the calibration coefficients, the condition of

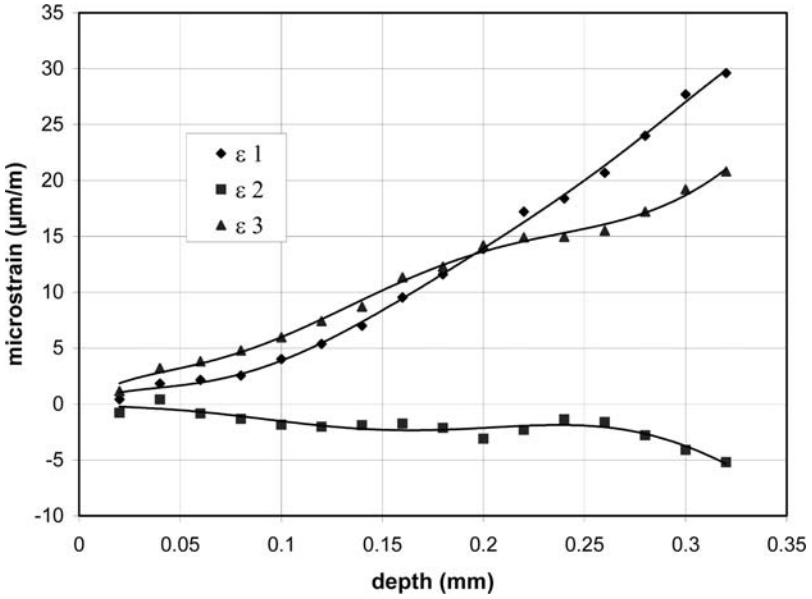

Fig. 8 Relaxation microstrains as measured by strain gauges 1, 2, and 3, interpolated with algebric polynomials functions of the sixth order

through-thickness hole, whose exact analytical solution is known (Ref 24) was simulated. Using Eq 9, the coefficient *B* was calculated for different values of the hole diameter. Results of the simulation are summarized and compared with the exact solution in Table 1. Average errors of less than 0.5% affect the calculated results.

In Fig. 9, the variation of the principal stress components σ_1 and σ_3 through the alumina coating thickness is illustrated; the minimum stress σ_3, approximately oriented according to the direction of the plasma torch translation, evidences a compression stress field along the whole coating thickness, assumable on the basis of a comparison among the thermal expansion coefficients of the alumina coating, of the NiAl bond coat and of the steel substrate. Compression stresses between −28 and −70 MPa were measured.

As a qualitative confirmation of the result, the value of the residual DTC stress of a ceramic coating deposited onto NiAl substrate and calculated on the basis of Eq 5 with the hypothesis of a thermal mismatch of about 150 °C between substrate and coating, gives a compression stress of about 41 MPa, not dissimilar from the measured values. As a further validation of the model used for the calibration of the experimental procedure, a simulation program was designed for the origination of residual stresses during the deposition of plasma sprayed coatings; results of the thermomechanical simulation, detailed and reported in Ref 31, evidenced a very good agreement with the experimental results obtained by the hole drilling method.

Finally, to direct attention to the degree of complexity of the developed model and to evaluate the quality and reliability of the obtained results, a more detailed analysis of the error was carried out in different scenarios (Fig. 10a-10d).

Figure 10 a shows the error that would affect the minimum stress at different depths if calculated with calibration coefficients determined without taking into account the discontinuities of elastic modulus and considering the examined structure as an homogeneous coating of alumina, thus underestimating the total

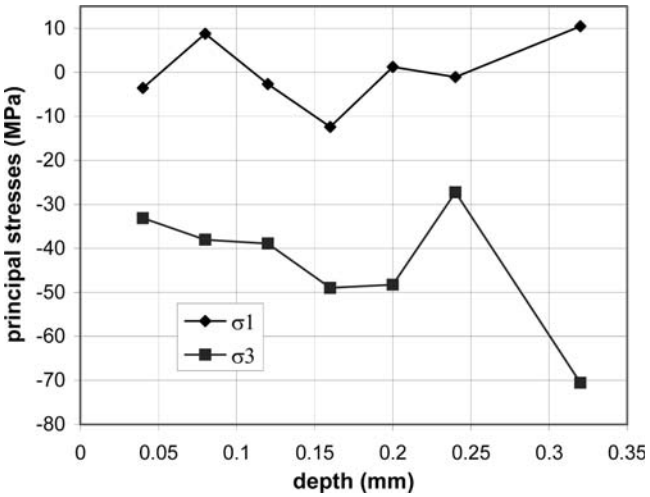

Fig. 9 Principal stresses (σ_1 and σ_3) calculated along coating thickness with 7 calculation steps

stiffness of the system. The error, increasing with increasing depth, can be quantified as about 20% of the stress value. Figure 10(b) shows the difference in the stress field calculated using the optimal distribution of calculation steps (7 steps of increasing width) and a distribution of 16 steps of constant width. A mismatch of more than 50% of the value can be noticed for most depths. The error related to the hole eccentricity is evaluated in Fig. 10(c); a correct determination of the hole eccentricity is guaranteed by the optical system mounted coaxially to the end mill. Eccentricities lower than 50 µm were measured, giving rise to a negligible error on the calculated stress (~1%). Finally, it is important to estimate the error induced as a consequence of the heating produced on drilling on the insulating sample, whose contribution cannot be conveniently accounted for by means of thermal balance strain gages. The ordinary procedure, set up for

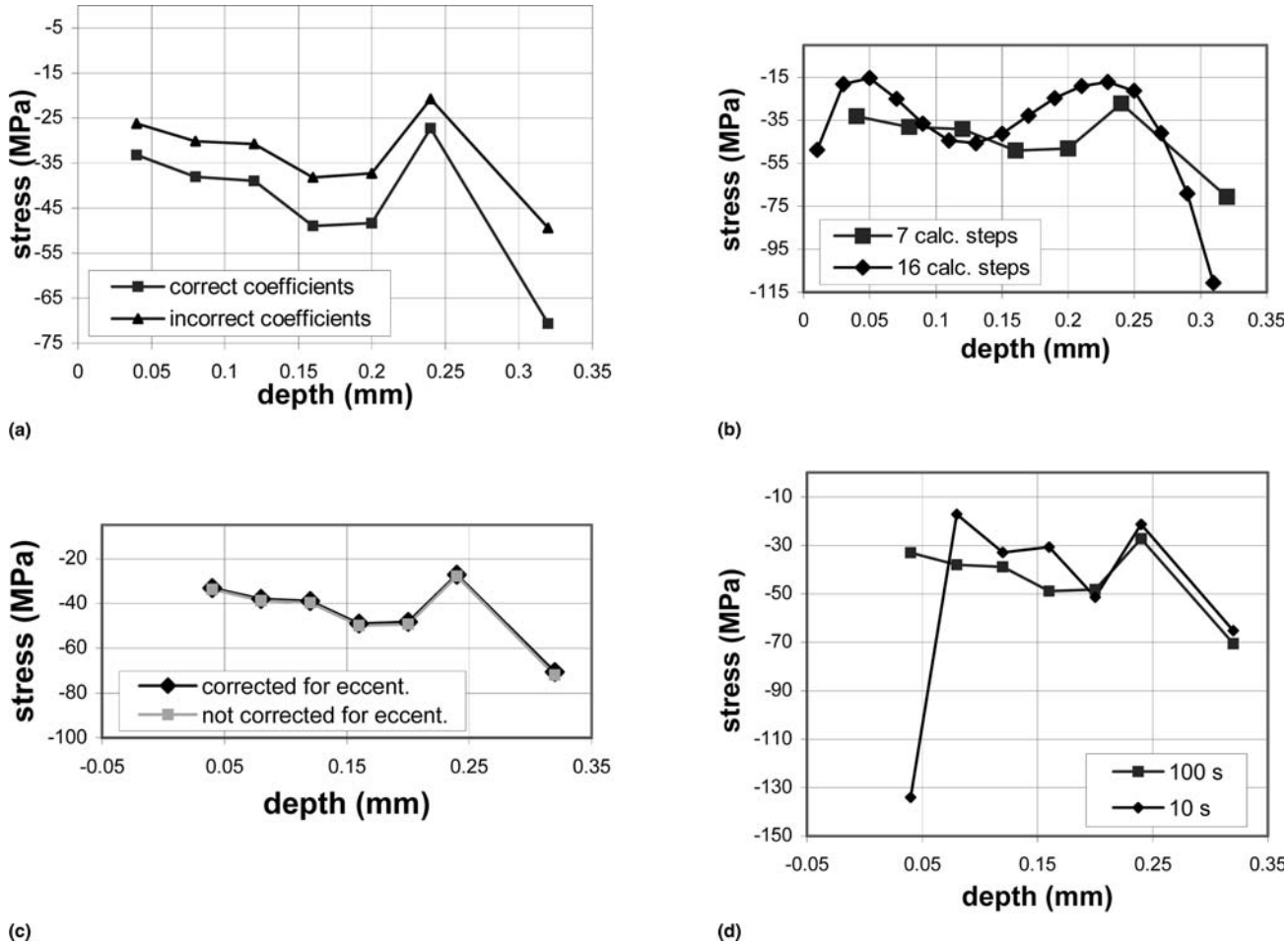

Fig. 10 Errors in the calculated residual stress (minimum stress): (a) caused by the use of incorrect calibration coefficients, (b) caused by nonoptimized number and width of calculation steps, (c) caused by eccentricity of the hole, and (d) caused by thermal strains generated on drilling

metals and other heat-conductive materials, was modified by introducing suitable time intervals (100 s) between the drilling steps, to allow for the extinction of the thermal component of the strain. Figure 10(d) compares results of the same test calculated using the values of strains measured after 100 s (modified conditions) or 10 s from drilling (normal conditions). Thermal strains induce sensible errors in the calculated stress, particularly evident in the most superficial layers of the coating.

6. Conclusions

The hole-drilling technique was applied and specifically developed for the measurement of residual stress fields in plasma sprayed ceramic coatings deposited on metal substrates with interposition of metallic bonding layers.

The analysis of composite layered structures required the implementation of an appropriate finite element model for the determination of the calibration coefficient to be used in the calculation of residual stresses from the measured relaxation strains.

The model was validated by simulating the case of through-thickness uniform stress distribution whose solution is analytically determinable, and negligible errors of the order of about 0.5% were estimated.

The influence of possible eccentricities of the machined hole, thermal effects caused on drilling as a consequence of the low thermal conductivity of the coatings, and the selection of different numbers of calculation steps was evaluated and quantified, thus identifying the correct conditions of the experimental procedure.

Results applied to the case of a 320 μm thick alumina coating plasma sprayed onto Ni20Al 180 μm thick bond coat and a carbon steel substrate showed the presence of a variable compressive stress field along coating thickness, whose main component ranges from about 25 to 70 MPa.

References

1. C. Godoy, E.A. Souza, M.M. Lima, and J.C.A. Batista, Correlation between Residual Stresses and Adhesion of Plasma Spayed Coatings: Effects of a Post-Annealing Treatment, *Thin Solid Films,* 2002, Vol 420-421, p 438-445
2. A. Nusair Khan, J. Lu, and H. Liao, Effect of Residual Stresses on Air Plasma Sprayed Thermal Barrier Coatings, *Surf. Coat. Technol.,* Vol 168 (No. 2-3), 2003, p 291-299
3. T.W. Clyne, Residual Stresses in Thick and Thin Surface Coatings, *En-*

cyclopaedia of Materials Science and Technology–Elasticity and Residual Stresses, P.J. Withers, Ed., Elsevier Science, London, UK, 2001, Section 4.1.
4. T.W. Clyne and S.C. Gill, Residual Stresses in Thermal Spray Coatings and Their Effect on Interfacial Adhesion: A Review of Recent Work, *J. Therm. Spray Technol.,* Vol 5 (No. 4), 1996, p 401-418
5. S. Kuroda and T.W. Clyne, The Quenching Stress in Thermally Sprayed Coatings, *Thin Solid Films,* Vol 200, 1991, p 49-66
6. J.A. Sue and G.S. Schajer, Stress Determination for Coatings, *Surface Engineering,* Vol 5, ASM Handbook, ASM International, 1994, p 647-653
7. F.A. Kandil, J.D. Lord, A.T. Fry, and P.V. Grant, A Review of Residual Stress Measurement Methods, A Guide to Technique Selection, NPL, Report MATC (A) 04, National Physical Laboratory, UK, 2001
8. P.J. Withers and H.K.D.H. Bhadeshia, Residual Stress, Measurement Techniques, *Mater. Sci. Technol.,* Vol 17 (No. 4), 2001, p 355-365
9. V. Teixeira, M. Andritschky, W. Fischer, H.P. Buchkremer, and D. Stover, Analysis of Residual Stresses in Thermal Barrier Coatings, *J. Mater. Proc. Technol.,* Vol 92-93, 1999, p 209-216
10. B. Elhamdi, J. Lu, and A. Lodini, Evaluation of Residual Stresses in Alumina Coating by Neutron Diffraction and the Incremental Holedrilling Method, *MAT-TEC'96,* J. Lu, Ed., IITT, Gournay sur Marne, France, 1996, p 89-98
11. M. Laribi, A.B. Vannes, N. Mesrati, and D. Treheux, Metallurgical Characterization and Determination of Residual Stresses of Coatings Formed by Thermal Spraying, *J. Therm. Spray Technol.,* Vol 12 (No. 2), 2003, p 234-239
12. Y.C. Yang and E. Chang, Residual Stress in Plasma-Sprayed Hydroxyapatite Coating Measured by the Material Removal Method, *J. Mater. Sci. Lett.,* Vol 22 (No. 13), 2003, p 919-922
13. J. Matejicek and S. Sampath, In Situ Measurement of Residual Stresses and Elastic Moduli in Thermal Sprayed Coatings. Part 1: Apparatus and Analysis, *Acta Mater.,* Vol 51 (No. 3), 2003, p 863-872
14. J. Matejicek, S. Sampath, D. Gilmore, and R. Neiser, In Situ Measurement of Residual Stresses and Elastic Moduli in Thermal Sprayed Coatings. Part 2: Processing Effects on Properties of Mo Coatings, *Acta Mater.,* Vol 51 (No. 3), 2003, p 873-885
15. M. Laribi, N. Mesrati, M. Laracine, A.B. Vannes, and D. Treheux, Experimental Determination of Residual Stresses in Materials Elaborated by Thermal Spraying, *Mater. Tech.* (Paris, France), Vol 89 (No. 9-10), 2001, p 15-21
16. D.J. Greving, E.F. Rybicki, and J.R. Shadley, Through-Thickness Residual Stress Evaluations for Several Industrial Thermal Spray Coatings Using a Modified Layer Removal Method, *J. Therm. Spray Technol.,* Vol 3 (No. 4), 1994, p 379-388
17. M.F.J. Koolloos and J.M. Houben, Residual Stresses in As-Sprayed and Heat Treated TBCs. Measurements and FEM Calculations, *Mater. Sci. Forum,* Vol 347-349, 2000, p 465-470
18. N. Baradel, L. Bianchi, F. Blein, A. Freslon, M. Jeandin, M. Ceretti, and J. Lu, Evaluation of Residual Stresses within Plasma Sprayed Zirconia (ZrO_2-Y_2O_3 8% wt) Coatings, *Thermal Spray: Meeting the Challenges of the 21st Century,* C. Coddet, Ed., May 25-29, 1998, Nice, France, ASM International, p 1623-1627
19. N.J. Rendler and I. Vigness, Hole Drilling Method of Measuring Residual Stresses, *Exp. Mech.,* Vol 6 (No. 12), 1966, p 577-586
20. Standard Test Method for Flexural Strength of Advanced Ceramics at Ambient Temperature, ASTM C1161-02c, ASTM International, West Conshohocken, PA
21. G.S. Schajer, Application of Finite Element Calculation to Residual Stress Measurement, *J. Eng. Mater. Technol.,* Vol 103, 1981, p 157-163
22. G.S. Schajer, Measurement of Non Uniform Residual Stress Using the Hole Drilling Method, *J. Eng. Mater. Technol.,* Vol 110 (No. 4), 1988, Part 1: 338-343, part 2: 345-349
23. G.S. Schajer and E. Altus, Stress Calculation Error Analysis for Incremental Hole Drilling Residual Stress Measurement, *J. Eng. Mater. Technol.,* Vol 118 (No. 1), 1996, p 120-126
24. G.S. Schajer, Use of Displacement Data to Calculate Strain Gauge Response in Non Uniform Stress Field, *Strain,* Vol 29 (No. 1), 1993, p 9-13
25. A. Zuccarello, Optimal Calculation Steps for the Evaluation of Residual Stress by the Incremental Hole Drilling Technique, *Exp. Mech.,* Vol 2, 1999, p 117-124
26. D. Vangi, Residual Stress Evaluation by the Hole Drilling Method with Off-Centre Hole: An Extension of the Integral Method, *J. Eng. Mater. Technol.,* Vol 119, 1997, p 79-85
27. M.T. Flaman, Brief Investigation of Induced Drilling Stresses in the Center-Hole Method of Residual Stress Measurement, *Exp. Mech.,* Vol 22, 1982, p 26-30
28. A.A. Scaramangas, R.F.D. Porter Goff, and R.H. Leggatt, On the Correction of Residual Stress Measurements Obtained Using the Center Hole Method, *Strain,* Vol 18, 1982, p 88-97
29. A. Ajovalasit, Measurement of Residual Stresses by the Hole-Drilling Method: Influence of Hole Eccentricity, *J. Strain Anal.,* Vol 14, 1979, p 171-178
30. D. Vangi, Data Management for the Evaluation of Residual Stresses by the Incremental Hole Drilling Method, *J. Eng. Mater. Technol.,* Vol 116 (No. 4), 1994, p 561-566
31. T. Valente, C. Bartuli, M. Sebastiani, and F. Casadei, Finite Element Analysis of Residual Stress in Plasma-Sprayed Ceramic Coatings, *Proc. Inst. Mech. Eng.,* Vol 218 *Part L: J. Materials: Design and Applications,* 2004, p 321-330